Proc. of the X Int. Conf. — Ion Implantation and other Applications of Ions and Electrons, Kazimierz Dolny 2014

Tailoring the Internal Evaporator for Effective Ion Beam Production — Volatile vs. Non-Volatile Substances

M. Turek*, A. Droździel, K. Pyszniak and S. Prucnal
Institute of Physics, Maria Curie-Skłodowska University, pl. M. Curie-Skłodowskiej 1, 20-031 Lublin, Poland

Two different designs of the internal evaporator in an arc discharge ion source are presented, suitable either for volatile, or high-melting point substances. A matter of the evaporator size and placement in order to obtain its appropriate temperature and, therefore, a stable and intense ion beam, is considered. Basic ion source characteristics, i.e. the dependences of ion current and discharge voltage on the discharge and filament currents as well as on the external magnetic field flux density are shown and discussed in order to find optimal working conditions. The results of measurements for both volatile (P, Zn, Se, S) and non-volatile (Pd) are presented, showing the applicability of the design for ion implantation purposes.

DOI: 10.12693/APhysPolA.128.939
PACS: 07.77.Ka, 34.80.Dp, 61.72.uj

1. Introduction

Arc discharge ion sources are widely used for needs of e.g. ion implantation and high-energy physics [1–5]. In order to fulfill a variety of demands, particular devices may differ by principle of operation, size and other aspects of design — more details could be found e.g. in [6, 7]. The arc discharge ion source with an internal evaporator [8–11] has become a basic tool for ion implantation in Lublin. It has been successfully used for both metallic and non-metallic ion beam production [12–16].

The method of internal evaporator heating using a hot cathode filament and arc discharge was also used in another design, based on a hollow cathode ion source [17]. The ion source proved to be especially suitable for the substances with a lower melting point (In, As, etc.) because of a larger distance between the evaporator and arc as well as the dominant role played by the filament heating. This was an inducement for testing different sizes as well as placements of the evaporator inside the ion source chamber [11] in order to obtain a proper evaporator temperature.

In the paper two different evaporator designs are discussed. One of them is suitable for high dose implantations of volatile elements like e.g. P, Zn, or Se, as the evaporator is much heavier than the standard one and its larger part is placed outside the chamber. This prevents from a premature deficiency of the feeding substance and enables a stable operation of the ion source. The other solution is intended rather for high melting point substances (Pd, Fe) as the shorter, thin-wall evaporator is almost totally placed inside the chamber, very near to the discharge area.

The construction and the principle of the ion source operation are briefly presented. Two different evaporator designs are considered. Basic characteristics of the ion source (dependences of ion current on the discharge and filament currents as well as on the magnetic field flux density inside the chamber) for both volatile (Zn, Se, P, and S) and non-volatile (Pd) substances are given and discussed.

2. Experimental

The construction of the ion source with an internal evaporator was described in detail in [8–11]. Here some basic facts are given for the sake of completeness. The discharge chamber is formed by an anode and two (front and rear) filament mounts. They are separated by insulators made of boron nitride. The chamber has the internal diameter of 11 mm and the length of ≈20 mm. A filament made of tungsten wire (a diameter of 0.75 mm) is placed inside the chamber. It surrounds the molybdenum evaporator. The evaporator potential is floating, as it is fixed using a boron nitride insulator. The filament is heated by the filament current I_c (typically 25–35 A). The typical voltage due to the cathode current flow is ≈7–10 V, the filament polarisation should be set in a way that ensures the acceleration of ions toward the extraction opening. The arc discharge burns between the anode and the cathode and is sustained by electron emission from the hot cathode. The discharge (anode) current I_a is usually set up to 4.5 A. The discharge voltage is typically maintained at 30–40 V. The discharge chamber is surrounded by the electromagnet coil. The external field is intended to partially compensate the magnetic field generated by the spiral cathode and to form the discharge plasma making the beam extraction as much effective as possible.

Ions produced in the arc discharge are extracted via the extraction hole having diameter of 0.8–1 mm using the voltage $V_{ext} = 25$ kV. The extracted beam is formed using a triple lens system and it passes a 90° sector separating magnet. The separated beam is accelerated by $V_{acc} = 75$ keV. Ion current is measured using a Faraday cup.

*corresponding author; e-mail: mturek@kft.ums.lublin.pl

3. Heating of the evaporator

The standard evaporator has a length of ≈27 mm and is placed mostly inside the chamber (≈15 mm of its length). Such a solution works very well for the substances with a moderate melting point like Al, Mn, Sb, etc. allowing production of stable ion beams for many hours. It was also useful for high melting point substances like Fe, Cr, V, and rare earth chlorides but requiring rather high discharge currents (naturally, the extracted currents were lower, up to ≈20 μA). On the other hand, the extracted currents were initially very high for volatile substances like In, As, P, etc. but high dose implantations were rather hard to do as the ion current decreased rapidly due to the excessive heating of the evaporator and shortage of the feeding substance.

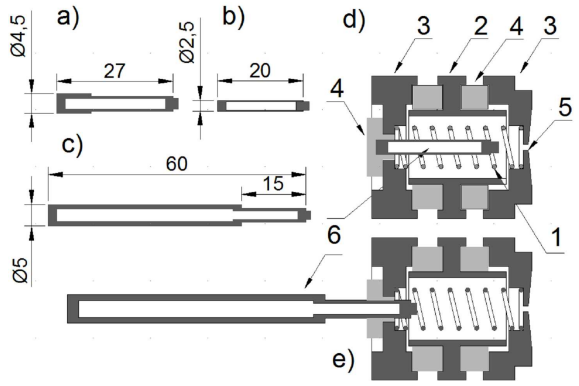

Fig. 1. Comparison of evaporators: a standard model (a), thin-wall evaporator for high melting point feeding substances (b), large evaporator for volatile substances (c). Schematic drawing of the ion source and placement of the evaporator in the case of non-volatile (d) and volatile (e) substances.

Hence, it was reasonable to follow two paths of the evaporator design: one suitable for volatile and the other for non-volatile substances. The designs are illustrated in Fig. 1. The evaporators used for volatile substances are almost twice longer than the standard ones and have thicker walls (1 mm or more). Only the tip of the evaporator (3–4 mm or more — the trial-and-error method was used) is heated by the discharge — most of it is outside the ionization chamber and is cooled down by the environment. On the other hand, the evaporator for high-melting point substances is shorter and thinner (a diameter of 2.5 mm) and its walls are as thin as possible (≈0.25 mm or less, but one should keep in mind that molybdenum is rather hard for machining). The evaporator could reach much higher working temperatures due to the fact that a major part of its surface is heated by the discharge.

A simple model of heating/cooling [18] of the evaporator could be applied in order to explain the reasons for different working temperatures in a more quantitative way. It is assumed that the environment has the same temperature T_e (which could be estimated as room temperature) in both cases. If a body of mass m and specific heat c is heated with the rate $\dot{Q}$, evolution of its temperature is described by the equation

$$\frac{\mathrm{d}T}{\mathrm{d}t} = \frac{\dot{Q}}{mc} - \frac{\alpha}{mc}\left(T - T_\mathrm{e}\right), \tag{1}$$

where α is a constant characterizing the cooling rate. Equation (1) has a solution of the form

$$T = T_\mathrm{e} + \frac{\dot{Q}}{\alpha}\left(1 - \exp\left(-\frac{\alpha t}{mc}\right)\right) \tag{2}$$

for T lower than the melting point. The equilibrium temperature

$$T_\mathrm{eq} = T_\mathrm{e} + \frac{\dot{Q}}{\alpha} \tag{3}$$

is achieved provided that the heating rate is too low to reach the melting point. The ratio of the temperature gains for both cases (the short and long evaporator) could be written as

$$x_\mathrm{sl} = \frac{T_\mathrm{eq(s)} - T_\mathrm{e}}{T_\mathrm{eq(l)} - T_\mathrm{e}} = \frac{\dot{Q}_\mathrm{s}\alpha_\mathrm{l}}{\dot{Q}_\mathrm{l}\alpha_\mathrm{s}}. \tag{4}$$

Heating and cooling rates depend on the evaporator geometry. There could be done a very rough approximation that both these rates are proportional to the surface of the evaporator contacting with the heater (discharge area) or the cooler (environment). Assuming that only the 5 mm long tip of the longer evaporator is heated while the rest of it is in the contact with the environment and that the 3/4 of the shorter evaporator is heated while the rest is cooled, one gets $x_\mathrm{sl} \approx 24$ which is a reasonable result (keeping in mind melting points of P or In).

4. Results

Ion source characteristics were determined when the stable working regime was achieved. Figure 2 shows the dependences of the separated ion currents of volatile substances (Zn, P, S, Se) on the discharge current I_a, when the other working parameters (e.g. I_c) were kept constant. One should keep in mind that in such case the amount of primary electrons (i.e. these emitted from the filament and contribute to the ion current indirectly) is constant, and the increase of I_a is mostly due to the increase in number of the electrons produced in collisions. Ion beams were produced using ion source in the configuration shown in Fig. 1e. For every substance increase of I_ion with I_a is observed due to the increase in evaporator temperature and number density of electrons and, hence, ionization probability. It is followed by the saturation of the $I_\mathrm{ion}(I_\mathrm{a})$ curve. The saturation can be caused by the increasing ion recombination probability as well as screening of the extraction field when the plasma density is growing. The increase of I_a is also accompanied by a rise of the discharge voltage. Maximal ion currents are 100 μA, 65 μA, 35 μA, and 20 μA for P, Zn, Se, and S, respectively.

Figure 3 shows the dependences of I_a and U_a on the filament current. In such case the ratio of primary and secondary (or environmental) electrons may change rapidly,

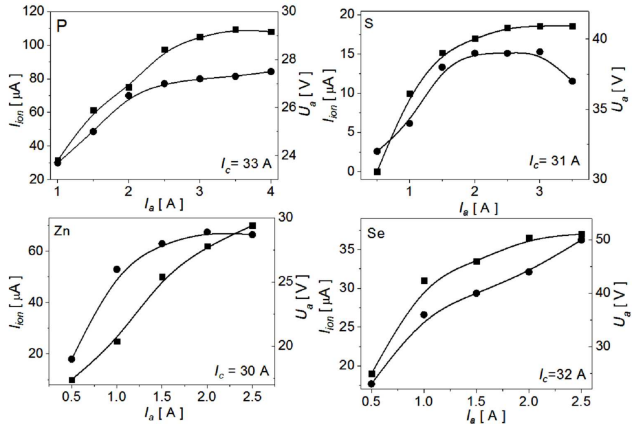

Fig. 2. Dependences of I_{ion} (squares) and U_{a} (circles) on the discharge current for volatile substances.

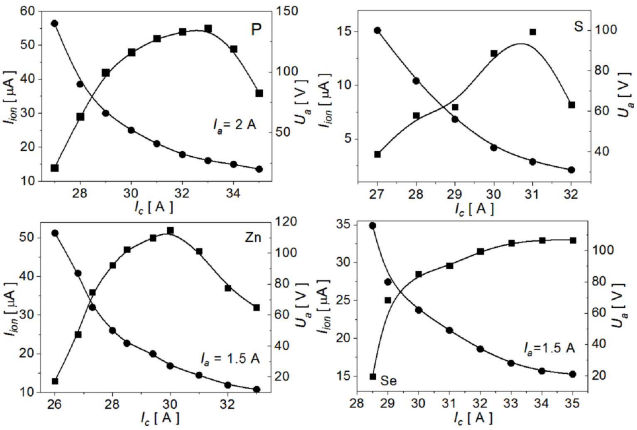

Fig. 3. As in Fig. 2, but for filament current for volatile substances.

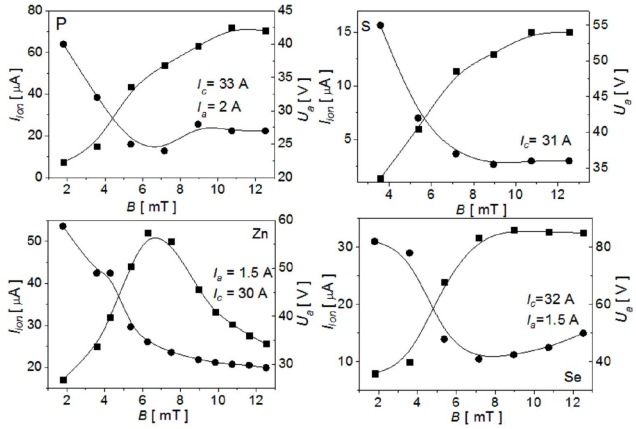

Fig. 4. As in Fig. 2, but for magnetic flux density from the external coil.

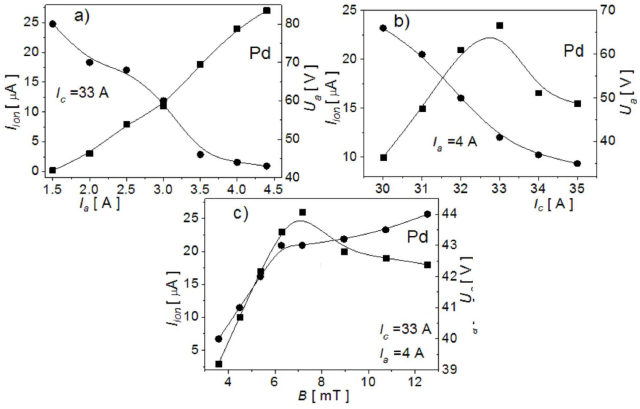

Fig. 5. Dependences of I_{ion} (squares) and U_{a} (circles) on the discharge current (a), filament current (b), and on magnetic flux density (c) for the non-volatile substance (Pd).

as the amount of primary electrons strongly depends on the I_{c}. A typical scenario is that the I_{ion} initially increases with I_{c} up to a certain level (as the electron density and vapour pressure rise), then degradation of the ion yield is observed. This could be due to the fact that U_{a} and, hence, electron energy decrease with the rising plasma density. One should remember that electron impact ionization cross-section dependences on energy have maxima for several eV. Therefore, the $I_{\mathrm{ion}}(U_{\mathrm{a}})$ and $I_{\mathrm{ion}}(I_{\mathrm{c}})$ curves demonstrate that trend. Maximal ion yields were observed for U_{a} in the range 20–40 V, in agreement with a rule-of-a-thumb saying that U_{a} should be 2–3 times larger than the ionization potential (in eV).

Dependences of I_{a} and U_{a} on the magnetic field flux density for the four considered volatile substances are shown in Fig. 4. In most of the cases rather high B values were required (above 10 mT) while for Zn one observes a quite narrow peak for lower field strength (near $B =$ 6 mT). This could be due to the fact that for Zn the optimal I_{c} was the lowest of all other cases. Hence, the weaker external magnetic field is required to compensate the field from the filament and push the plasma near the extraction opening.

The same characteristics were also measured using the ion source in the configuration shown in Fig. 1d, i.e. suitable for a non-volatile substance. Measurements were done for Pd (melting point at ≈1555 °C). Figure 5a shows that high discharge currents are required in order to heat the evaporator and obtain an intense ion beam. One should also notice that no saturation of $I_{\mathrm{ion}}(I_{\mathrm{a}})$ is observed in that case. The ion current of ≈25 μA was achieved. The $I_{\mathrm{ion}}(I_{\mathrm{c}})$ curve (see Fig. 5b) has a maximum at $I_{\mathrm{c}} = 33$ A. It corresponds to $U_{\mathrm{a}} = 45$ V, which is larger than U_{a} for volatile substances (the evaporator is also heated by the filament that surrounds it). The $I_{\mathrm{ion}}(B)$ curve is presented in Fig. 5c. The optimal value of B for Pd ions production is 7 mT. One observes increase of U_{a} with B for non-volatile Pd as a feeding substance, while for all volatile substances the trend was opposite.

The ion source ability to provide an intense and stable ion beam was also tested. The exemplary results (for Zn) are shown in Fig. 6. Note that the beam ion current increased when correction of working conditions was made after ≈90 min of operation. One can see that the beam

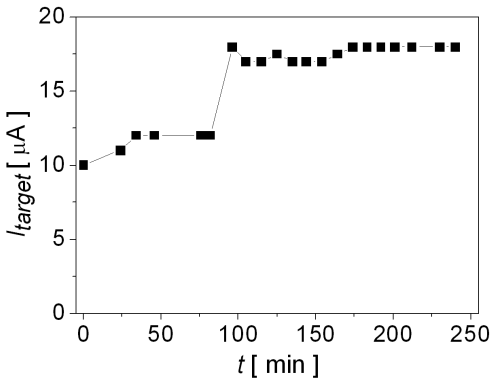

Fig. 6. Ion current (Zn^+) measured on the target as a function of time.

intensity is sufficient to perform high fluence implantation ($\approx 5 \times 10^{16}$ cm^{-2} or even more) within a single operating cycle. Similar results were obtained for P. For Se and S the ion current intensity decreased after 1–1.5 h of operation. However, implantations with fluences of 5×10^{15} cm^{-2} are feasible.

5. Conclusions

Two different designs of arc discharge ion source with the evaporator were considered: one suitable for volatile substances, while the other intended for high melting point ones. The proposed solutions differ mainly by the size of the evaporator and its placement. In the first solution only the tip is heated, which results in a relatively low temperature of the long evaporator placed outside the discharge chamber. Such a heating mode allows maintaining a stable feeding substance vapour pressure. There were obtained ion currents of 100 μA, 65 μA, 35 μA, and 20 μA for P, Zn, Se, and S, respectively. The second design involves a small evaporator almost totally immersed in the discharge, which leads to very high working temperatures of the evaporator. Such a solution seems suitable for non-volatile substances and was tested using metallic Pd. Ion current of 25 μA of Pd^+ was obtained. Basic characteristics of the ion source in both configurations were measured in order to find optimal working conditions. In most cases of volatile substances $I_a = 2$ A is a good starting point (discharge current is usually increased during ion source operation). The discharge voltage should be maintained in the range 20–40 V by adjusting I_c. In the case of non-volatile substances, as high as possible I_a is usually required.

The presented solutions enable implantations with the fluences 10^{16}–5×10^{16} cm^{-2} within a single working cycle for substances like P, Zn, In, Cu. For Se or S feasible fluences are smaller by an order of magnitude.

References

[1] I.G. Brown, B. Feinberg, J.E. Galvin, *J. Appl. Phys.* **63**, 4889 (1988).

[2] A.I. Ryabchikov, S.V. Dektjarev, I.B. Stepanov, *Rev. Sci. Instrum.* **65**, 3126 (1994).

[3] S.P. Bugaev, A.G. Nikolaev, E.M. Oks, P.M. Schanin, G.Yu. Yushkov, *Rev. Sci. Instrum.* **65**, 3119 (1994).

[4] L. Penescu, R. Catherall, J. Lettry, T. Stora, *Rev. Sci. Instrum.* **81**, 02A906 (2010).

[5] P.P. Deichuli, A.A. Ivanov, N.V. Stupishin, *Rev. Sci. Instrum.* **79**, 02C106 (2008).

[6] I.G. Brown, *The Physics and Technology of Ion Sources*, Wiley, Weinheim 2004.

[7] I.G. Brown, E. Oks, *IEEE Trans. Plasma Sci.* **33**, 1931 (2005).

[8] M. Turek, S. Prucnal, A. Droździel, K. Pyszniak, *Rev. Sci. Instrum.* **80**, 043304 (2009).

[9] M. Turek, A. Droździel, K. Pyszniak, S. Prucnal, J. Żuk, *Przeglad Elektrotechniczny* **86**, 193 (2010).

[10] M. Turek, S. Prucnal, A. Droździel, K. Pyszniak, *Nucl. Instrum. Methods Phys. Res. B* **269**, 700 (2011).

[11] M. Turek, A. Droździel, K. Pyszniak, S. Prucnal, D. Mączka, Yu. Yushkevich, A. Vaganov, *Instrum. Exp. Techn.* **55**, 469 (2012).

[12] S. Prucnal, M. Turek, A. Drozdziel, K. Pyszniak, S.Q. Zhou, A. Kanjilal, W. Skorupa, J. Zuk, *Appl. Phys. B* **101**, 315 (2010).

[13] S. Prucnal, M. Turek, A. Drozdziel, K. Pyszniak, A. Wojtowicz, S.Q. Zhou, A. Kanjilal, A. Shalimov, W. Skorupa, J. Zuk, *Centr. Europ. J. Phys.* **9**, 338 (2011).

[14] S. Prucnal, S.-Q. Zhou, X. Ou, H. Reuther, M.O. Liedke, A. Mücklich, M. Helm, J. Zuk, M. Turek, K. Pyszniak, W. Skorupa, *Nanotechnology* **23**, 485204 (2012).

[15] P. Węgierek, P. Billewicz, *Acta Phys. Pol. A* **123**, 948 (2013).

[16] T. Wilczyńska, R. Wiśniewski, P. Konarski, *Przegląd Elektrotechniczny* **88**, 292 (2012) (in Polish).

[17] M. Turek, A. Droździel, K. Pyszniak, S. Prucnal, *Nucl. Instrum. Methods Phys. Res. A* **654**, 57 (2011).

[18] J. O'Connell, *Phys. Teach.* **37**, 551 (1999).